Mater Renew Sustain Energy (2015) 4:9
DOI 10.1007/s40243-015-0052-y

REVIEW PAPER

# Fractional-order models of supercapacitors, batteries and fuel cells: a survey

**Todd J. Freeborn**[1] · **Brent Maundy**[2] · **Ahmed S. Elwakil**[3]

Received: 22 March 2015 / Accepted: 28 May 2015 / Published online: 14 June 2015


**Abstract** This paper surveys fractional-order electric circuit models that have been reported in the literature to best fit experimentally collected impedance data from energy storage and generation elements, including super-capacitors, batteries, and fuel cells. In all surveyed models, the employment of fractional-order capacitors, also known as constant phase elements, is imperative not only to the accuracy of the model but to reflect the physical electrochemical properties of the device.

**Keywords** Impedance spectroscopy · Constant phase element · Super-capacitors · Batteries · Fuel cells

## Introduction

Modeling of energy storage and generation elements used in hybrid and renewable energy sources is crucial for future development of these sources [1]. Of specific importance are super-capacitors, batteries and fuel cells [2]. A survey of published fractional-order models has been carried out and is presented in this work. These models provide best fit to experimentally measured impedances and/or transient responses and employ one or more constant phase element (CPEs) [3]; also known as the fractional-order capacitor [4].

✉ Ahmed S. Elwakil
elwakil@ieee.org

Todd J. Freeborn
todd.freeborn@gmail.com

[1] Department of Electrical and Computer Engineering, University of Alabama, Box 870286, Tuscaloosa, USA

[2] Department of Electrical and Computer Engineering, University of Calgary, 2500 University Dr. N.W, Calgary, Canada

[3] Department of Electrical and Computer Engineering, University of Sharjah, P.O. Box 27272, Sharjah, UAE

From a circuit theory perspective, it is possible to define a general frequency-domain electrical impedance which is proportional to $s^{\alpha}; s = j\omega$. This device is known as a fractance [5] from which classical circuit elements are special cases of the general device when the order $\alpha$ is $-1$, 0, and 1 for a capacitor, resistor, and inductor, respectively. A CPE (or fractional-order capacitor) is characterized by the impedance $Z_{CPE} = (1/C_{\alpha})s^{\alpha}$; where $C_{\alpha}$ is termed pseudo-capacitance with units F/sec$^{(1-\alpha)}$, and $\alpha$ is the order. These units were originally proposed in [6]. A CPE has a phase angle, $\phi_{CPE} = \alpha\pi/2$ which is constant, independent of frequency and dependent only on the order $\alpha$. While $\alpha \in \Re$ is mathematically possible, the values from experimentally collected data of CPEs are in the range of $0 < \alpha \leq 1$; therefore, it has also become known as a fractional-order capacitor.

A number of recent surveys and special issues have focused on the applications of fractional-order circuits and systems in general [7] and particularly in industrial automation [8]. Meanwhile, energy storage components and particularly electrochemical double-layer capacitors [9] [fabricated to provide high and very high capacitances (super-capacitors)], as well as batteries are critical components in hybrid energy systems which require accurate models for these devices [10]. Although there exists a considerable mass of research on the modeling of these devices, a survey focusing on fractional-order models has not been conducted. It is the purpose of this paper to fill this gap.

## Super-capacitor models

Super-capacitors, also referred to as ultra-capacitors or electric double-layer capacitors, are electrical energy storage devices with applications in diverse scales from energy

storage for wind turbines [11, 12], renewable energy sources [13], hybrid and electric vehicles [14], biomedical sensors [15] to wireless sensor nodes [16]. Traditionally, these elements have been modeled using RC networks to describe their behavior over wide frequency bands, with larger frequency bands requiring a greater number of parameters [17]. However, recent work has employed the concept of fractional impedances to model and describes the behavior of these components [9]. Fractional models have been investigated for applications that include:

- Impedance modeling of nickel finer mesh for simulation and design of elements in pulse power systems [18];
- Modeling high power performance to characterize super-capacitor capabilities [19];
- Modeling the impedance of super-capacitors over finite frequency bands to reduce the required model parameters [20–22];
- Modeling the transient characteristics from very small (seconds) [23] to very large (months) timescales [24];
- Measurement of fractional characteristics from transient behavior [25, 26];
- Modeling and control of super-capacitor systems using fractional state-space models [27] and fractional linear systems [28, 29];
- Implementation in a buck–boost converter for power electronics [30].

A simple super-capacitor model derived from the porous electrode behavior of super-capacitors is shown in Fig. 1a. This model comprises a series resistor, $R_0$, and a CPE [31] with an impedance given by

$$Z(s) = R_0 + \frac{1}{C_1 s^{\alpha_1}}. \tag{1}$$

This model has been used in [19] to model the impedance in the frequency range from 10 mHz to 1000 Hz and [20] in the frequency range 50–215 mHz with $\alpha_1 \approx 1$ and 450 mHz to 100 Hz with $\alpha_1 \approx 0.5$. It was also used in [26] to model the transient characteristics of commercial super-capacitors to a voltage-step input signal. For example, the step responses of 3 different 1F rated super-capacitors in the test circuit shown in Fig. 2a to an input step of 5 V are given in Fig. 2b. From the experimental datasets, the parameters of each super-capacitor model were found using a least-squares fitting applied to the step response:

$$v_o(t) = 5\left[\frac{t^{\alpha_1}}{C_1(R+R_0)} E_{\alpha_1,\alpha_1+1}\left(\frac{-t^{\alpha_1}}{C_1(R+R_0)}\right)\right]. \tag{2}$$

where $v_o(t)$ is the time domain output voltage and $E_{a,b}(\cdot)$ is the two-term Mittag-Leffler function defined as [3]

$$E_{a,b}(z) = \sum_{k=0}^{\infty} \frac{z^k}{\Gamma(ak+b)}. \tag{3}$$

Using least-squares fitting, the parameters of three commercial super-capacitors (KR, PM and BP) being modeled using Fig. 2a were extracted yielding $(C_1, R_0, \alpha_1)$ = (0.1, 10, 0.53), (0.87, 0.46, 0.97) and (0.69, 0.07, 0.97), respectively. As evident from the extracted values of $\alpha_1$, two of the three super-capacitors possess parameters very close to those expected by normal capacitors with $\alpha_1$ very close to unity and capacitance values within the expected tolerances. However, the KR super-capacitor has

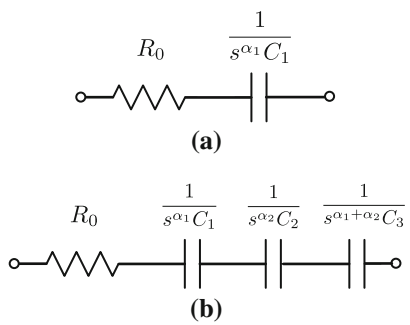


**Fig. 1** Models representing the impedance of a super-capacitor with **a** a single CPE and **b** three CPEs

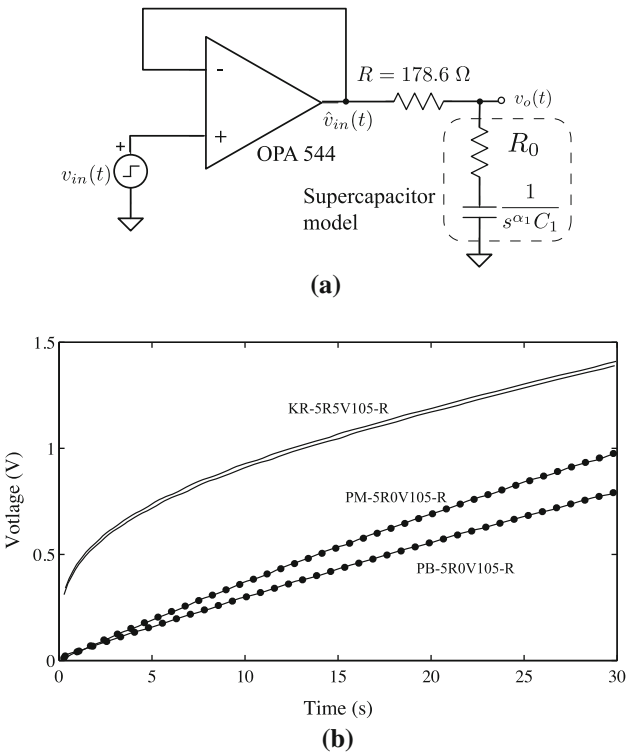


**Fig. 2** **a** Step-response test circuit and **b** measured and simulated step responses to a 5 V input collected from 1F rated capacitors from Cooper-Bussmann with part numbers KR-5R5V105-R, PM-5R0V105-R, and PB-5R0V105-R

($\alpha_1 \approx 0.53$) indicating that it would be incorrect to assume the behavior of this capacitor being typical of a normal capacitor. Although all three super-capacitor are marketed with a 1F rated capacitance, the KR model has very different charging characteristics than both the PM and PB models, as seen in Fig. 2b.

Another fractional model is given in Fig. 1b, which is composed of a series resistor and three CPEs. The impedance of this model is given by:

$$Z(s) = R_0 + \frac{1}{C_1 s^{\alpha_1}} + \frac{1}{C_2 s^{\alpha_2}} + \frac{1}{C_3 s^{(\alpha_1+\alpha_2)}}. \quad (4)$$

This model was used to represent the behavior of an HE0120C-0027A 120F super-capacitor in the frequency band 1 mHz–1 kHz [22]. This model is unique in that the order of the third CPE with impedance $1/C_3 s^{(\alpha_1+\alpha_2)}$ is greater than 1, with a value of $\alpha_1 + \alpha_2 = 0.2848 + 0.866 = 1.1508$ reported in [22], which has not previously been explored in literature.

The models given in Fig. 1 can be expanded [20] to include a fractional zero which may provide a better fit to experimental data than the all-pole models for some super-capacitors. The impedance of this model is given by

$$Z(s) = R_0 + k\frac{(1 + s/\omega_0)^{\alpha}}{s^{\beta}}. \quad (5)$$

A simulated Nyquist impedance plot is shown in Fig. 3 using parameters extracted from EPCOS 5F super-capacitors (P/N: B49100-A1503-Q) [20]. The fractional behavior is obvious when compared to an ideal capacitor, which would appear as a vertical line on this plot, i.e., a pure imaginary impedance. The emergence of two zones, above and below $Re(Z) \approx 0.22\,\Omega$, differentiates the super-capacitor from ideal capacitors and is attributed to the diffusion effect and electrode porosity [20]. This fractional behavior is frequently attributed throughout literature to the complex internal structure and electrochemical processes of the super-capacitors [9, 20].

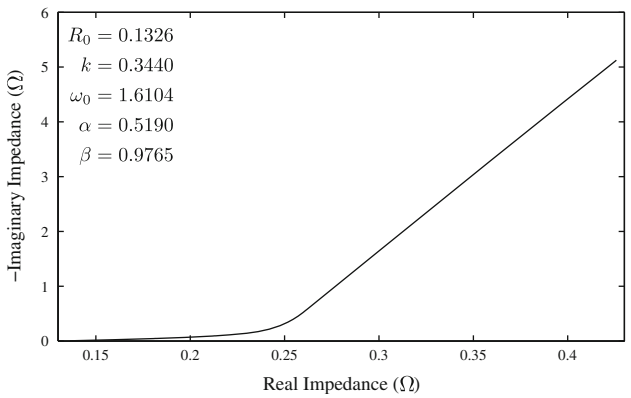


**Fig. 3** Simulated Nyquist plot of (5) using extracted fractional parameters from [20]

## Battery models

Batteries are energy generation elements that are ubiquitous in the modern world. They are present in nearly every portable electronic system and every vehicle providing electricity from the microamps scale to the amps scale. Batteries generate their electricity from a multitude of different chemistries that are commercially available. Some of the most widely popular chemistries include lead-acid, nickel-cadmium, and lithium-ion/lithium-polymer. Like super-capacitors, fractional-order circuit models have been employed to model the impedance of batteries because they show the best fit with experimental data and typically require fewer parameters than their integer-order counterparts. These fractional models have been investigated for applications that include:

- Modeling the impedance of lead-acid [32], nickel/metal hydride [33], and lithium-ion batteries [34, 35] in finite frequency bands;
- Determining the relationship between fractional-order model parameters and state-of-charge of nickel-cadmium [36], lithium-ion [37–39], alkaline [40], lead-acid [41] batteries;
- Designing high-power batteries based on the fractional contribution of the elements to total polarization [42];
- State-of-health estimations based on parameters measured during the cranking function of lead-acid batteries in vehicles [43, 44].

To represent the equivalent impedance of batteries; three examples with increasing complexity are given in Fig. 4a–c.

The model given in Fig. 4a was proposed in [35] as a reference model for modeling the battery dynamics for the purpose of improving battery monitoring. This model is composed of four circuit elements including an inductor, two resistors, and a CPE with equivalent impedance given by:

$$Z(s) = sL_0 + R_0 + \frac{R_1}{s^{\alpha_1} R_1 C_1 + 1}. \quad (6)$$

The model was used to fit experimental data collected in the frequency range 100 mHz–5 kHz from a commercially available lithium-polymer battery produced by Kokam [35] resulting in a significant reduction in the inaccuracy of the battery's dynamic voltage response.

The model given in Fig. 4b was used in [36] to determine the dependence of the state-of-charge of sealed nickel-cadmium cells on model parameters and has also

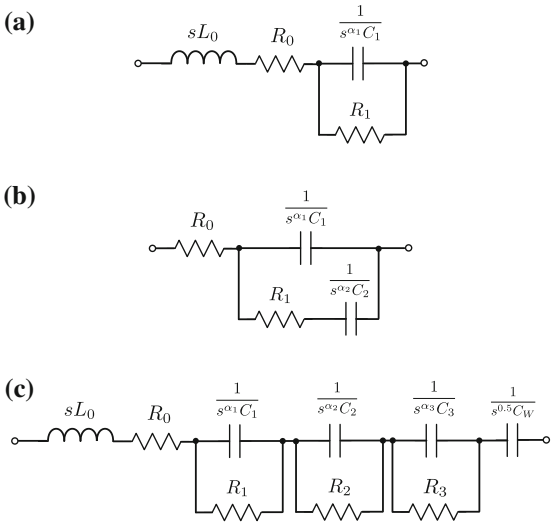


**Fig. 4** Models of battery impedance for **a** lithium-ion cells, **b** nickel-cadmium cells, and **c** high-power lithium cells

been used in [34] to study lithium-ion batteries. This model incorporates four circuit elements; two resistors and two CPEs with impedance given by:

$$Z(s) = R_0 + \frac{1 + s^{(\alpha_1+\alpha_2)}R_1C_2}{s^{(\alpha_1+\alpha_2)}C_1C_2R_1 + s^{\alpha_1}C_1 + s^{\alpha_2}C_2}, \tag{7}$$

where, in [36], $R_0$ represents the ohmic resistance, $R_1$ the charge transfer resistance, $\{C_1, \alpha_1\}$ the double-layer capacitance, and $\{C_2, \alpha_2\}$ the Warburg element (a CPE with $\alpha = 0.5$). This model was used to fit experimental data collected from approximately 2 mHz–250 Hz. The study found that with increasing state-of-charge, the ohmic and charge transfer resistances decreased and the double-layer capacitance increased, potentially providing a mechanism for estimating/monitoring the state-of-charge by measuring these fractional model parameters. Finally, the model given in Fig. 4c was proposed in [42] to analyze DC polarization to aid in the design of high-power cells. This model incorporates nine circuit elements, including an inductor, four resistors, three CPEs and a Warburg impedance with an impedance given by:

$$Z(s) = sL_0 + R_0 + \frac{1}{s^{0.5}C_W} + \sum_{i=1}^{n=3} \frac{R_i}{s^{\alpha_i}R_iC_i + 1}. \tag{8}$$

This model was used in [42] to fit data collected from 10 mHz to 100 kHz. The simulated impedance of (8) using parameters from [42] for a fresh battery is given in Fig. 5. The three parallel *R*/CPE branches were introduced to model arcs in high and intermediate frequency ranges, which the authors commented could be due to the reaction in the solid electrolyte interface and the interfacial charge transfer reaction combined with the electrical double-layer capacitive behavior.

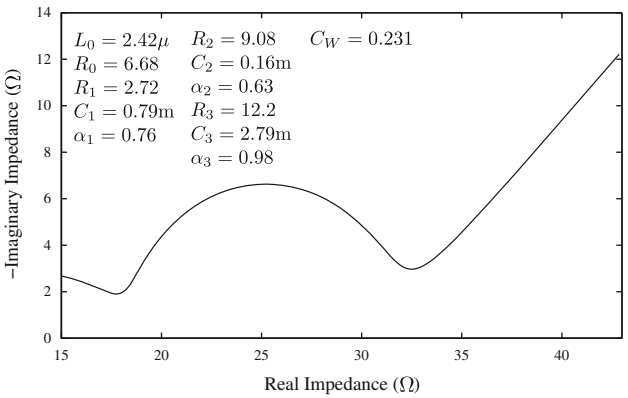


**Fig. 5** Simulated Nyquist plot of (8) using extracted fractional parameters from [42]

## Fuel cell models

Fuel cells are energy generation elements that convert chemical energy into electricity and hold the promise of high efficiency and low pollution for applications including transportation and stationary electricity generation for domestic, commercial and industrial sectors [45]. There are multiple types of fuel cell technologies that are being pursued that include proton exchange membrane fuel cells (PEMFCs), solid oxide fuel cells (SOFCs), direct methanol fuel cells (DMFCs), and microbial fuel cells (MFCs) to name a few. Circuit models have also recently been applied to these elements, having been investigated for applications including:

- Monitoring the state-of-health of a PEMFC with respect to the water content of the membrane electrode assembly [46, 47];
- Analyzing the reaction kinetics and interfacial characteristics of an anode in a DMFC [48];
- Characterizing the output power dynamics of a SOFC for management by a control system [49];
- Monitoring the anode colonization by electrode-reducing micro-organisms in an MFC [50].

Three fuel cell models are shown in Fig. 6a–c.

The model given in Fig. 6a was presented in [46] to monitor the state-of-health of the fuel cell with respect to the water content of the membrane electrode assembly. The proposed model incorporates two fractional elements, a CPE and a Warburg impedance. In this model, $R_m$ represents the ohmic resistance of the electrolyte, $R_p$ represents the polarization resistance due to the oxygen reduction reaction, $\{C_1, \alpha_1\}$ represent the double-layer capacitance at the electrode/electrolyte interface, and $C_2$ represents a Warburg diffusion element. The impedance of this circuit is given as:

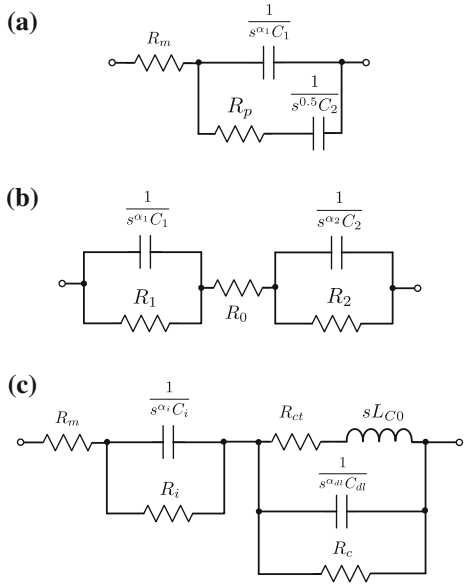


**Fig. 6** Circuits models for the impedance of a **a** proton exchange membrane fuel cell (PEMFC), **b** solid oxide fuel cell (SOFC) and **c** direct methanol fuel cell (DMFC)

$$Z(s) = R_m + \frac{1}{s^{\alpha_1}C_1 + \left(1/\left(R_p + 1/(s^{0.5}C_2)\right)\right)}. \tag{9}$$

This fractional model is accurate over a wide range of the fuel cell operating conditions with the resistances showing high sensitivity to the flooding or drying of the PEMFC membrane electrode assembly. Therefore, monitoring these parameters provides a means of detecting the state-of-hydration of the fuel cell; which is important because fuel cells require a steady water content in the electrolyte for efficient operation. The model given in Fig. 6b was presented in [49] to improve the control design for load-following using model predictive control; which requires an accurate dynamic model. The model incorporates two CPEs to account for the behavior of the anode and cathode of the fuel cell in addition to $R_0$, which represents the electrolyte resistance, $\{R_1, R_2\}$ which represent activation resistance of the anode and cathode, respectively, and $\{C_1, \alpha_1, C_2, \alpha_2\}$ which define the impedance of the electrical double layer. The impedance of this circuit is:

$$Z(s) = \frac{R_1}{1 + R_1C_1s^{\alpha_1}} + R_0 + \frac{R_2}{1 + R_2C_2s^{\alpha_2}}. \tag{10}$$

Using this model, parameters were estimated from experimental impedance data in the frequency band from 100 mHz to 100 kHz. The simulated impedance plot using the parameters from [49] is given in Fig. 7. The contribution of the two CPEs is clearly seen as the overlapping arcs at low and high frequencies. This model was further used in [49] to design a control system for the management of fuel cell output power.

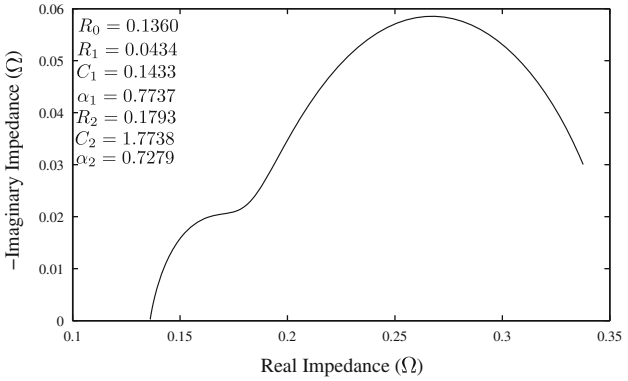


**Fig. 7** Simulated impedance plot of (10) using extracted fractional parameters from [42]

The model given in Fig. 6c was presented in [48] to model and analyze the reaction kinetics and interfacial characteristics of an anode in a DMFC. The circuit models the impedance of the fuel cell membrane, interface, and catalyst layers; incorporating two CPEs to account for the behavior of the anode–membrane interface and catalyst layer of the fuel cell. In this model, $R_m$ represents the membrane resistance while the interface impedance is modeled by a parallel combination of a resistor ($R_i$) and a CPE defined by an admittance constant ($Q_i = 1/C_i$) and order ($\alpha_i$). The catalyst layer is modeled by a parallel combination of a resistor ($R_c$), a CPE defined by an admittance constant ($Q_{\mathrm{dl}} = 1/C_{\mathrm{dl}}$) and order ($\alpha_{\mathrm{dl}}$), and a series branch with resistance ($R_{\mathrm{ct}}$) along with an inductance ($L_{\mathrm{C0}}$). The total impedance of this circuit is given by $Z(s) =$

$$R_m + \frac{R_i}{1 + R_iQ_is^{\alpha_i}} + \frac{R_c\left(R_{\mathrm{ct}}^2 + s^2\right)}{1 + R_c\left[R_{\mathrm{ct}} - sL_{\mathrm{C0}} + Q_{\mathrm{dl}}s^{\alpha_{\mathrm{dl}}}\right]}. \tag{11}$$

The experimental results from 5 mHz to 10 kHz were fit with less than 1 % relative error, confirming the model accuracy. In [48], the authors concluded that the use of CPEs supported the simulation of realistic reaction conditions with porous electrode and rough interface structures and improved the fit of experimental data over a wider frequency range than using a model with the traditional circuit elements.

## Conclusion

We have surveyed published fractional-order circuit models that best fit experimentally collected impedance data of super-capacitors, batteries, and fuel cells. All surveyed models rely on using at least one fractional-order capacitor in an attempt to accurately capture the underlying electrochemical dynamics. This survey should also serve to

bridge the gap between the wide employment of fractional-order impedances in bio-chemistry and their much less employment in circuit design.



## References

1. Bauman, J., Kazerani, M.: A Comparative Study of Fuel-Cell–Battery, Fuel-Cell–Ultracapacitor, and Fuel-Cell–Battery–Ultracapacitor Vehicles. IEEE Trans. Vehicular Tech. **57**(2), 760–769 (2008)
2. Khaligh, A., Li, Z.: Battery, Ultracapacitor, Fuel Cell, and Hybrid Energy Storage Systems for Electric, Hybrid Electric, Fuel Cell, and Plug-In Hybrid Electric Vehicles: State of the Art. IEEE Trans. Vehicular Tech. **59**(6), 2806–2814 (2010)
3. Ortigueira, M.D.: Fractional Calculus for Scientists and Engineers. Springer, Heidelberg (2011)
4. Elwakil, A.S.: Fractional-Order Circuits and Systems: An Emerging Interdisciplinary Research Area. IEEE Circuits Syst. Mag. **10**(4), 40–50 (2010)
5. Nakagawa, M., Sorimachi, K.: Basic characteristics of a fractance device, IEICE Trans. Fundam. Electron. Commun. Comput. Sci., E 75, pp. 1814–1819 (1992)
6. Westerlund, S., Ekstam, L.: Capacitor theory. IEEE Trans. Dielectr. Electr. Insul. **1**(5), 826–839 (1994)
7. Elwakil, A.S., Maundy, B.J., Fortuna, L., Chen, G.: Guest Editorial: Fractional-order circuits and systems, IEEE. J. Emerging Sel. Top. Circuits Syst. **3**(3), 297–300 (2013)
8. Efe, M.O.: Fractional order systems in industrial automation—a survey. IEEE Trans. Ind. Inf. **7**(4), 582–591 (2011)
9. Martin, R., Quintana, J.J., Ramos, A., Nuez, I.: "Modeling electrochemical double layer capacitor, from classical to fractional impedance. In: IEEE Mediterr. Electrotechnical Conf, pp. 61–66 (2008)
10. Rodrigues, S., Munichandraiah, N., Shukla, A.K.: "AC impedance and state-of-charge analysis of a sealed lithium-ion rechargeable battery. J. Solid State Electrochem. **3**(7–8), 397–405 (1999)
11. Abbey, C., Joos, G.: "Super-capacitor energy storage for wind energy applications. IEEE Trans. Ind. Appl. **43**(3), 769–776 (2007)
12. Jayasinghe, S.D., Vilathgamuwa, D.M.: Flying supercapacitors as power smoothing elements in wind generation. IEEE Trans. Ind. Electron. **60**(7), 2909–2918 (2013)
13. Pegueroles-Queralt, J., Bianchi, F.D., Gomis-Bellmunt, O.:"A Power Smoothing System Based on Supercapacitors for Renewable Distributed Generation. IEEE Trans. Ind. Electron. doi:10.1109/TIE.2014.2327554 (2014)
14. Cao, J., Emadi, A.: "A new battery/ultracapacitor hybrid energy storage system for electric, hybrid, and plug-in hybrid electric vehicles. IEEE Trans. Power Electron. **27**(1), 122–132 (2012)
15. Pandey, A., Allos, F., Hu, A., Budgett, D.: "Integration of supercapacitors into wirelessly charged biomedical sensors. In: IEEE Int. Symp. Ind. Electron., pp. 56–61 (2011)
16. Kim, S., No, K., Chou, P.: "Design and performance analysis of super-capacitor charging circuits for wireless sensor nodes, IEEE. J. Emerging Sel. Top. Circuits Syst. **1**(3), 391–402 (2011)
17. Shi, L., Crow, M.: "Comparison of ultracapacitor electric circuit models. In: IEEE Power and Energy Society General Meeting, pp. 1–6 (2008)
18. Cahela, D.R., Tatarchuk, B.J.: "Impedance modeling of nickel fiber/carbon fiber composite electrodes for electrochemical capacitors". In: Int. Conf. Ind. Electron. Control Instrum., pp. 1080–1085 (1997)
19. Mahon, P.J., Paul, G.L., Keshishian, S.M., Vassallo, A.M.: "Measurement and modeling of the higher-power performance of carbon-based super-capacitors. J. Power Sources **91**(1), 68–76 (2000)
20. Quintana, J.J., Ramos, A., Nuez, I.: Identification of the fractional impedance of ultra-capacitors. In: Proc. 2nd AFAC Workshop Fractional Differ. Appl., pp. 289–293 (2006)
21. Dzieliński, A., Sarwas, G., Sierociuk, D.:"Comparison and validation of integer and fractional order ultracapacitor models. Adv. Diff. Equ. (2011). doi:10.1186/1687-1847-2011-11
22. Martynyuk, V., Ortigueira, M.: Fractional model of an electrochemical capacitor. Signal Process. (2014). doi:10.1016/j.sigpro.2014.02.021
23. Bertrand, N., Briat, B., Vinassa, J.M., ElBrouji, E.H.: "Influence of relaxation process on super-capacitor time response, Eur. Conf. Power Electron. Appl., pp. 1–8 (2009)
24. Wang, Y.: "Modeling Ultracapacitors as Fractional-Order Systems, in New Trends in Nanotechnology and Fractional Calculus Applications. In: Baleanu, D., et al. (eds.) pp. 257–262. Springer, Netherlands (2010)
25. Dzieliński, A., Sarwas, G., Sierociuk, D.: "Time domain validation of ultracapacitor fractional order model. In: IEEE Conf. Decis. Control, pp. 3730–3735 (2010)
26. Freeborn, T.J., Maundy, B., Elwakil, A.S.: "Measurement of super-capacitor fractional-order model parameters from voltage-excited step response, IEEE. J. Emerging Sel. Top. Circuits Syst **3**(3), 367–376 (2013)
27. Dzieliński, A., Sierociuk, D.: "Ultracapacitor modeling and control using discrete fractional order state-space model. Acta Montanistica Slovaca **13**(1), 136–145 (2008)
28. Bertrand, N., Sabatier, J., Briat, O., Vinassa, J.: "Fractional nonlinear modeling of ultra-capacitors. Commun. Nonlinear Sci. Numer. Simulat., vol. 15, no. 5, pp. 1327–1337 (2010)
29. Bertrand, N., Sabatier, J., Briat, O., Vinassa, J.M.: Embedded fractional nonlinear super-capacitor model and its parametric estimation method. IEEE Trans. Ind. Electron. **57**(12), 3991–4000 (2010)
30. Parreno, A., Roncero-Sanchez, P., del Toro Garcia, X., Feliu, V., Castillo, F.: Analysis of the Fractional Dynamics of an Ultracapacitor and Its Application to a Buck-Boost Converter. In: New Trends in Nanotechnology and Fractional Calculus Applications, pp. 97–105. Springer, Netherlands (2010)
31. Kotz, R., Carlen, M.: "Principles and applications of electrochemical capacitors. Electrochim. Acta **45**(15–16), 2483–2498 (2000)
32. Nelatury, S.R., Singh, P.: Extracting equivalent circuit parameters of lead-acid cells from sparse impedance measurements. J. Power Sources **112**(2), 621–625 (2002)
33. Nelatury, S.R., Singh, P.: Equivalent circuit parameters of nickel/metal hydride batteries from sparse impedance measurements. J. Power Sources **132**(1–2), 309–314 (2004)
34. Liao, X., Yu, J., Gao, L.: Electrochemical study on lithium iron phosphate/hard carbon lithium-ion batteries. J. Solid State Electrochem. **16**(2), 423–428 (2012)
35. Waag, W., Sauer, D.U.: Application-specific parameterization of reduced order equivalent circuit battery models for improved accuracy at dynamic load, Meas., vol. 46, no. 10, pp. 4085–4093 (2013)
36. Viswanathan, V., Salkind, A.J., Kelley, J.J., Ockerman, J.B.: "Effect of state of charge on impedance spectrum of sealed cells part I: Ni-Cd cells. J. Appl. Electrochem. **25**(8), 716–728 (1995)

37. Rodrigues, S., Munichandraiah, N., Shukla, A.K.: AC impedance and state-of-charge analysis of a sealed lithium-ion rechargeable battery. J. Solid State Electrochem. **3**(7–8), 397–405 (1999)
38. Xu, J., Mi, C.C., Cao, B., Cao, J.: A new method to estimate state of charge of lithium-ion batteries based on the battery impedance model. J. Power Sources **233**(1), 277–284 (2013)
39. Waag, W., Sauer, D.U.: Adaptive estimation of the electromotive force of the lithium-ion battery after current interruption for an accurate state-of-charge and capacity determination. Appl. Energy **111**, 416–427 (2013)
40. Rodrigues, S., Munichandraiah, N., Shukla, A.K.: AC impedance and state-of-charge analysis of alkaline zinc/manganese dioxide primary cells. J. Appl. Electrochem. **30**(3), 371–377 (2000)
41. Sabatier, J., Aoun, M., Oustaloup, A., Gregoire, G., Ragot, F., Roy, P.: Fractional system identification for lead acid battery state of charge estimation. Signal Process. **86**(10), 2645–2657 (2006)
42. Kang, D.K., Shin, H.C.: "Investigation on cell impedance for high-power lithium-ion batteries. J. Solid State Electrochem. **11**(10), 1405–1410 (2007)
43. Sabatier, J., Cugnet, M., Laruelle, S., Grugeon, S., Sahut, B., Oustaloup, A., Tarascon, J.M.: "A fractional order model for lead-acid battery crankability estimation, Commun. Nonlinear Sci. Numer. Simulat., vol. 15, no. 5, pp. 1308–1317 (2010)
44. Cugnet Sabatier, M., Laruelle, S., Grugeon, S., Sahut, B., Oustaloup, A., Tarascon J.: On lead-acid battery resistance and cranking-capability estimation. In: IEEE Trans. Ind. Electron., vol. 57, no. 3, pp. 909–917 (2010)
45. Jiang, W., Fahimi, B.: Active current sharing and source management in Fuel Cell-Battery hybrid power system. IEEE Trans. Ind. Electron. **57**(2), 752–761 (2010)
46. Fouquet, N., Doulet, C., Nouillant, C., Dauphin-Tanguy, G., Ould-Bouamama, B.: Model based PEM fuel cell state-of-health monitoring via ac impedance measurements. J. Power Sources **159**(2), 905–913 (2006)
47. Gebregergis, A., Pillay, P., Rengaswamy, R.: PEMFC fault diagnosis, modeling, and mitigation. IEEE Trans. Ind. Appl. **46**(1), 295–303 (2010)
48. Hsu, N.Y., Yen, S.C., Jeng, K.T., Chien, C.C.: Impedance studies and modeling of direct methanol fuel cell anode with interface and porous structure perspectives. J. Power Sources **161**(1), 232–239 (2006)
49. Deng, Z., Cao, H., Li, X., Jiang, J., Yang, J., Qin, Y.: Generalized predictive control for fractional order dynamic model of solid oxide fuel cell output power. J. Power Sources **195**(24), 8103–8907 (2010)
50. Martin, E., Savadogo, O., Guiot, S.R., Tartakovsky, B.: "Electrochemical characterization of anodic biofilm development in a microbial fuel cell. J. Appl. Electrochem **43**(5), 533–540 (2013)